ResearchGate

See discussions, stats, and author profiles for this publication at: https://www.researchgate.net/publication/50364555

Cyclooxygenase reaction mechanism of prostaglandin H synthase from deuterium kinetic isotope effects

ARTICLE *in* JOURNAL OF INORGANIC BIOCHEMISTRY · MARCH 2011

Impact Factor: 3.44 · DOI: 10.1016/j.jinorgbio.2010.11.015 · Source: PubMed

CITATIONS
14

READS
31

5 AUTHORS, INCLUDING:

Gang Wu
University of Texas Health Science Center at …
30 PUBLICATIONS **462** CITATIONS
SEE PROFILE

Ah-Lim Tsai
University of Texas Health Science Center at …
142 PUBLICATIONS **4,604** CITATIONS
SEE PROFILE

Available from: Ah-Lim Tsai
Retrieved on: 25 January 2016

NIH Public Access
Author Manuscript
J Inorg Biochem. Author manuscript; available in PMC 2012 March 1.

Published in final edited form as:
J Inorg Biochem. 2011 March 1; 105(3): 264–272. doi:10.1016/j.jinorgbio.2010.11.015.

CYCLOOXYGENASE REACTION MECHANISM OF PROSTAGLANDIN H SYNTHASE FROM DEUTERIUM KINETIC ISOTOPE EFFECTS

Gang Wu[a], **Jian-Ming Lü**[b], **Wilfred A. van der Donk**[c], **Richard J. Kulmacz**[a], and **Ah-lim Tsai**[a,*]

[a] Department of Internal Medicine, University of Texas Health Science Center at Houston, Houston, TX 77030

[c] Department of Chemistry, University of Illinois at Urbana-Champaign, Urbana, IL 61801

Abstract

Cyclooxygenase catalysis by prostaglandin H synthase (PGHS) is thought to involve a multistep mechanism with several radical intermediates. The proposed mechanism begins with transfer of the C13 *pro-(S)* hydrogen atom from the substrate arachidonic acid (AA) to the Tyr385 radical in PGHS, followed by oxygen insertion and several bond rearrangements. The importance of the hydrogen-transfer step to controlling the overall kinetics of cyclooxygenase catalysis has not been directly examined. We quantified the non-competitive primary kinetic isotope effect (KIE) for both PGHS-1 and -2 using unlabeled AA and several deuterated AAs, including 13-*pro*-*(S)* d-AA, 13,13-d_2-AA and 10, 10, 13,13-d_4-AA. The primary KIE for steady-state cyclooxygenase catalysis, $^{D}k_{cat}$, ranged between 1.8 and 2.3 in oxygen electrode measurements. The intrinsic KIE of AA radical formation by C13 *pro-(S)* hydrogen abstraction in PGHS-1 was estimated to be 1.9–2.3 using rapid freeze-quench EPR kinetic analysis of anaerobic reactions and computer modeling to a mechanism that includes slow formation of a pentadienyl AA radical and rapid equilibration of the AA radical with a tyrosyl radical, NS1c. The observation of similar values for steady-state and pre-steady state KIEs suggests that hydrogen abstraction is a rate-limiting step in cyclooxygenase catalysis. The large difference of the observed KIE from that of lipoxygenase indicates very different mechanism of hydrogen transfer.

1. INTRODUCTION

Prostaglandin H synthase (PGHS), both PGHS-1 and PGHS-2, exhibits two distinct, yet interrelated enzymatic activities: a peroxidase activity and a cyclooxygenase activity. The peroxidase activity generates a high-oxidation state intermediate, Intermediate I, which contains a ferryl heme and a proto-porphyrin radical; intra-molecular electron transfer from Tyr385 to the ferryl heme yields Intermediate II and a Tyr385 radical [1–3]. This tyrosyl radical initiates the cylcooxygenase cycle of PGHS, which converts arachidonic acid (AA) to the cyclooxygenase product, PGG_2 [4,5]. PGG_2 is itself a peroxidase substrate, and can

*Corresponding Author. Telephone: 713-500-6771. Ah-lim.Tsai@uth.tmc.edu.
[b]Current address: Michael E. DeBakey Department of Surgery, Baylor College of Medicine, Houston, TX 77030

Publisher's Disclaimer: This is a PDF file of an unedited manuscript that has been accepted for publication. As a service to our customers we are providing this early version of the manuscript. The manuscript will undergo copyediting, typesetting, and review of the resulting proof before it is published in its final citable form. Please note that during the production process errors may be discovered which could affect the content, and all legal disclaimers that apply to the journal pertain.

NIH-PA Author Manuscript
NIH-PA Author Manuscript
NIH-PA Author Manuscript

NIH-PA Author Manuscript

NIH-PA Author Manuscript

NIH-PA Author Manuscript

dissociate to activate another PGHS molecule in an auto-accelerative process that can produce a rapid burst of potent lipid signaling molecules [2].

Hamberg and Samuelsson proposed a cyclooxygenase reaction mechanism that starts with removal of the *pro-(S)* hydrogen at C13, as outlined in Scheme 1 [6,7]. As noted above, the enzyme oxidant responsible for this hydrogen abstraction is now known to be the Tyr385 radical (Tyr371 in PGHS-2), and the initial lipid intermediate is a pentadienyl radical, with spin density distributed between C11–C15 (step A). Addition of O_2 at C11 is thought to generate the first peroxyl radical intermediate (step B). The next step is formation of an endoperoxide between C11 and C9, which transfers the radical to C8 (step C). Subsequent cyclization between C8 and C12 forms a cyclopentane ring and delocalizes the radical over C13–C15 (step C), and reaction with a second O_2 at C15 produces a PGG_2 radical (step D). Finally, back transfer of a hydrogen from Tyr385 regenerates the Tyr385 radical and produces PGG_2 (step F), which dissociates from the protein and leaves the enzyme ready to start the next cyclooxygenase cycle. Although this mechanism is supported by almost all the experimental evidence [4,5], most of the mechanistic details remain untested. For example, resolved EPR signatures have been determined only for the Tyr385 radical in PGHS-1 (and Tyr 371 in PGHS-2) and AA pentadienyl radical intermediates in PGHS-2 [8–10]. The AA pentadienyl radical accumulates when PGHS-2 is reacted anaerobically with peroxide and AA, permitting the AA radical to be characterized by EPR [8–10]. In contrast, PGHS-1 reacted under similar conditions leads to accumulation of other radical species [11]; these include NS1c, which is a tyrosyl radical rather than an AA-based radical (Tsai et al., accompanying paper in this issue). These recent results suggested that an AA-based radical is an intermediate between the initial Tyr385 radical and NS1c in PGHS-1, but a direct test of this proposal was lacking.

A major issue regarding the cyclooxygenase mechanism is the relative importance of the various steps in setting the overall catalytic rate. Few direct measurements have been made for individual steps in the mechanism in Scheme 1, and a rate constant has been evaluated only for the step involving formation of the Tyr385 radical [12,13]. Hamberg and Samuelsson used an analysis of isotope enrichment in unreacted substrate after cyclooxygenase reaction with tritium-substituted 8, 11, 14-eicosatrienoic acid to conclude that the initial hydrogen abstraction from substrate (step A, Scheme 1) was rate limiting [7]. However, results from a recent study of competitive oxygen isotope effects in PGHS-1 cyclooxygenase catalysis appeared to identify the first kinetically irreversible step as formation of the endoperoxide ring or the bicyclic intermediate (steps C and D, Scheme 1); hydrogen abstraction from fatty acid appeared to be reversible [14].

The present study was designed to test whether an AA-based radical was indeed an intermediate in NS1c formation in PGHS-1 and to obtain an independent assessment of the kinetic importance and reversibility of the initial hydrogen abstraction step in cyclooxygenase catalysis. In contrast to the indirect, competitive method with a crude seminal vesicle homogenate used in the pioneering experiments [7], we used purified PGHS-1 and -2 to directly determine the primary deuterium KIE of cyclooxygenase catalysis by a non-competitive method with specific-deuterated substrates. Conversion of AA to PGG_2 involves multiple steps, precluding direct determination of the intrinsic KIE of the C13 *pro-(S)* hydrogen abstraction step from overall cyclooxygenase reaction rates. To overcome this difficulty we used rapid-freeze quench EPR (RFQ-EPR) to analyze the kinetics of PGHS-1 reacting with peroxide and unlabeled or 13, 13-d_2-AA under anaerobic conditions, which prevented proceeding beyond step A in Scheme 1. Although the kinetic events turned out to be more complicated than expected, we were able to estimate the intrinsic KIE of C13 *pro-(S)* hydrogen abstraction by fitting the experimental data to a mechanism with slow formation of AA radical and faster conversion of AA radical to the

NIH-PA Author Manuscript

NIH-PA Author Manuscript

NIH-PA Author Manuscript

NS1c tyrosyl radical. The results of these KIE studies with steady-state and transient kinetic methods provide new mechanistic insights into the cyclooxygenase reaction.

2. EXPERIMENTAL PROCEDURES

2.1 Materials

Hemin was purchased from Sigma (St. Louis, MO) and Porphyrin Products (Logan, UT). EtOOH was either purchased from Polysciences Inc. (Warrington, PA) or kindly provided by Dr. G. Barney Ellison (University of Colorado, Boulder, CO); the EtOOH concentration was determined from the A_{230} using a molar absorptivity of 43 $mM^{-1}cm^{-1}$[15]. Tween 20 was from Anatrace (Maumee, OH). Arachidonic acid was purchased from Nu-Chek Prep, Inc. (Elysian, MN). The 13-*pro*-(*S*) d_1-AA, 13, 13-d_2-AA and 10, 10, 13, 13-d_4-AA were synthesized in high stereochemical and isotopic purity as described earlier [16–19].

PGHS-1 and -2 holoenzymes were prepared as previously published procedure as detailed in the accompany paper (Tsai et al., accompanying paper in this issue) [20]. The concentrations of PGHS-1 and -2 holoenzymes were calculated from their A_{410} using an extinction coefficient of 165 $mM^{-1}cm^{-1}$[21]. Cyclooxygenase activity was routinely assayed polarographically at 30 °C with a YSI Model 5331 electrode (with a standard membrane) and a YSI Model 53 monitor [22]. The reaction mixture contained 3.0 ml of 0.1 M KPi, pH 7.2 with 1.0 mM phenol and 0.05% Tween 20. PGHS-1 preparations had cyclooxygenase k_{cat} values for AA consumption of 65–100 s^{-1} (assuming 2 mol O_2/mol AA). Cyclooxygenase k_{cat} values for the PGHS-2 preparations averaged ~ 15 s^{-1}.

2.2 Non-competitive steady-state KIE measurement

The non-competitive steady-state KIE was calculated as the ratio of AA conversion rates (determined from O_2 consumption) with unlabeled and deuterated AAs as substrate. Either standard or high sensitivity O_2 electrode membranes were used. The temperature was controlled by an Isotemp 3016 water circulator (Fisher Scientific). Reactions were started by injection of enzyme; unless otherwise indicated, the enzyme concentration was 5 – 10 nM for PGHS-1 and 10 nM for PGHS-2. Working stocks of unlabeled and deuterated AAs were prepared by evaporating the organic solvent with a stream of N_2 gas and resuspending the fatty acid in 0.1 M Tris, pH 8.5 buffer. The AA concentrations of the working stocks were determined from the extent of O_2 consumption in reactions with excess PGHS-1, assuming 2 mol O_2/mol AA. The values of k_{cat} and K_M were obtained by fitting rate vs. [substrate] data to the Michaelis-Menten equation:

$$v=k_{cat}[\mathrm{PGHS}][\mathrm{AA}]/([\mathrm{AA}]+K_M). \quad \text{[Eq. I]}$$

Primary KIE values were calculated as follows:

$$^{\mathrm{D}}k_{cat}=k_{cat,\mathrm{H}}/k_{cat,\mathrm{D}}; \quad \text{[Eq. II]}$$

$$^{\mathrm{D}}K_M=K_{M,\mathrm{H}}/K_{M,\mathrm{D}}; \quad \text{[Eq. III]}$$

$$^{\mathrm{D}}(k_{cat}/K_M)=(k_{cat}/K_M)_{\mathrm{H}}/(k_{cat}/K_M)_{\mathrm{D}}. \quad \text{[Eq. IV]}$$

NIH-PA Author Manuscript

NIH-PA Author Manuscript

NIH-PA Author Manuscript

2.3 Measurement of deuterium oxide solvent isotope effect

PGHS-1 cyclooxygenase rates were determined at 30 °C in 0.1 M KP_i buffer at different pH values prepared in H_2O or in 90% D_2O/10% H_2O. The concentration of AA was 70 μM and a high sensitivity electrode membrane was used. The buffer pH was determined using a VWR Scientific model 8000 pH meter. The pD values of the 90% D_2O buffers were calculated as [23]:

$$\mathrm{pD}=\mathrm{pH}+0.004\times\text{percentage of}\,\mathrm{D_2O}. \qquad \text{[Eq. V]}$$

2.4 Determination of deuterium KIEs by RFQ-EPR pre-steady state kinetic measurements

An anaerobic mixture of PGHS-1 with AA or 13, 13-d_2-AA was prepared by injecting a concentrated anaerobic solution of the fatty acid in EtOH into an anaerobic solution of PGHS-1 in 0.1M KP_i, pH 7.2, containing 10% glycerol and 0.1% Tween 20. The final concentrations were 30 μM for PGHS-1, 150 μM for the fatty acid, and 6.2 % for EtOH. For the kinetic experiments, the PGHS-1/fatty acid mixture was reacted with an equal volume of buffer containing 150 μM EtOOH using an Update Instrument (Madison, WI) System 1000 chemical/freeze quench apparatus with a Model 1019 syringe ram and a Model 715 controller. The mixing apparatus was inside an anaerobic chamber (Coy Laboratory Products, Inc.) filled with 10% H_2 in N_2 and fitted with a palladium-based O_2 scrubber. The ram velocity was 2 cm/s, the nozzle was 0.008 inch and the dead time was ~4 ms [24]. Single-push mixing was used for reactions < 160 ms; longer reactions used a push-push protocol. Reactions were conducted at room temperature (23 °C). RFQ-EPR procedures have been described previously [24].

After an EPR spectrum was acquired for each of the freeze-trapped kinetic samples, two approaches were used to analyze the changes in EPR spectrum with reaction time. In the first approach (spectral deconstruction), the NS1c component was resolved from the composite EPR spectrum by subtraction of residual WD1 signal. The fraction of residual WD1, *f*, was calculated by simultaneously satisfying two conditions over the relevant range of magnetic field:

$$(S_{exp} - S_{cal}) \approx 0 \qquad \text{[Eq. VI]}$$

$$S_{cal}=f * S_{WD1}+(1-f) * S_{NS1c} \qquad \text{[Eq. VII]}$$

S_{cal} and S_{exp} are the calculated and observed EPR spectra, respectively; S_{WD1} and S_{NS1c} are the EPR signals of pure WD1 and NS1c, respectively. In the second step, formation and decay rates for the NS1c radical signal were estimated by fitting the time course of the resolved NS1c spin concentration to the following equation:

$$I=I_0 * k_{NS1c}[\exp(-k_{NS1c} * t) - \exp(-k_{decay} * t)]/(k_{decay} - k_{NS1c}), \qquad \text{[Eq. VIII]}$$

where I and I_0 are the observed and the maximum intensities of the NS1c radical signal; k_{NS1c} and k_{decay} (with unit s^{-1}) are the observed NS1c radical formation and decay rates, respectively.

The second approach to analyzing each set of RFQ-EPR spectra used global analysis with the Pro-K algorithm (Applied Photophysics, Leatherhead, UK) to resolve the EPR signals of

NIH-PA Author Manuscript

NIH-PA Author Manuscript

NIH-PA Author Manuscript

individual intermediates in a specified input mechanism. Formation of the WD1 signal from Tyr385· was rapid and complete by 32 ms, with only one or two time points collected, so the kinetics of this step were not resolved. Further, no radical signal other than WD1 and NS1c accumulated to a noticeable level during these reactions. Accordingly, time points before 32 ms were excluded, and global analysis used a two step reaction model beginning with WD1:

$$\text{WD1 radical} \xrightarrow{k_i} \text{NS1c radical} \xrightarrow{k_{ii}} \text{EPR silent species} \qquad \text{[Eq. IX]}$$

The KIE for conversion of WD1 to NS1c, ^{D}k, was calculated from the ratio of value of k_i (obtained from global analysis) k_{NS1c} (obtained from spectral deconstruction) with AA as substrate and the corresponding k_i or k_{NS1c} value with 13, 13-d_2-AA as substrate.

2.5 EPR spectroscopy

EPR spectra were recorded at 110–120 K on a Bruker EMX spectrometer at ~ 9.2 gHz with modulation frequency = 100 kHz, modulation amplitude = 2 G, time constant = 327 ms and microwave power = 1 mW. Spin concentrations were determined by double integration of the EPR signals [11]. A packing factor of 0.45 was used for quantification of RFQ-EPR samples [24].

2.6 Computer modeling

The SCoP program (Simulation Resources Inc., Redlands, CA) was used to simulate the kinetics of tyrosyl and fatty acid radicals during anaerobic reaction of EtOOH with PGHS-1 pre-equilibrated with AA or 13, 13-d_2-AA based on the model in Scheme 2 and the rate constants described below. Reaction 2 in Scheme 2 was considered to transfer spin to either Tyr348 (a good candidate due to its location near the C13 *pro-(S)* hydrogen of AA) or to Tyr385', which is proposed to have a different phenyl ring orientation from that in Tyr385· giving the WD1 EPR signal (Tsai et al., accompanying paper in this issue). Hyperconjugation between the p_z orbital of C1 and the two Cβ protons is presumed to be greater for Tyr385· than for Tyr385'; thus the tyrosyl radical has a more "relaxed" conformation in NS1c than in WD1. The level of AA used for pre-equilibration with PGHS-1 in the RFQ-EPR experiments (75 μM) was well above the K_M for fatty acid, ensuring saturation of the PGHS active site. Accordingly, the AA binding process was not included in the simulation and every reaction step was treated as an intra-molecular, first-order hydrogen transfer (or proton-coupled electron transfer). The level of EtOOH used (150 μM) ensured that formation of Tyr385· was much faster than hydrogen abstraction from fatty acid and was not rate-limiting. Accordingly, formation of Tyr385· was omitted from the model.

Reactions using AA and 13, 13-d_2-AA were distinguished in the simulation by different values of k_1 (and of k_2 when NS1c was generated). The value of k_1 was 20 s^{-1} for AA and was varied between 1 and 10 s^{-1} for 13, 13-d_2-AA. The value of k_2 was varied between 50 and 1000 s^{-1}. The experimentally determined value, 0.08 s^{-1}, was used for k_3. The k_{-2} value was set much smaller than that of k_2 because the equilibrium between AA radical and NS1c appeared to strongly favor NS1c. As long as k_2 was $\gg k_1$, and $k_{-1} < k_2$, variation of k_{-1} between 0 and 5 s^{-1} did not affect the kinetic simulations (data not shown). Accordingly, the value of k_{-1} was subsequently set to zero. Quenching of the radical was assumed to be irreversible.

NS1c formation kinetics predicted by simulation were fitted to a single exponential function:

NIH-PA Author Manuscript

NIH-PA Author Manuscript

NIH-PA Author Manuscript

$$I = I_0 * [1 - \exp(-k_{pred} * t)]. \quad \text{[Eq. X]}$$

The predicted KIE value was calculated as the ratio of k_{pred} values from simulations with AA and 13, 13-d_2-AA as substrate. The theoretical intrinsic KIE of the hydrogen abstraction step in the simulations (i.e., hydrogen abstraction from AA by Tyr385·) was the ratio of the k_1 values used for AA and 13, 13-d_2-AA.

3. RESULTS

3.1 Non-competitive, steady-state KIE for PGHS cyclooxygenase catalysis

Cyclooxygenase k_{cat} and K_M values were calculated from the substrate dependence curves of PGHS-1 and -2 in steady state reactions with AA, 13-*pro*-(*S)* d-AA, 13, 13-d_2-AA or 10, 10, 13, 13-d_4-AA at 20 °C and pH 7.2. Simple, saturable kinetics were observed in each case. A typical steady-state Michaelis-Menten plot, for PGHS-2 with AA and 13, 13-d_2-AA, is presented in Fig. 1; Table 1 shows the k_{cat} and K_M values determined in the steady-state reactions and the KIEs calculated from them. The $^{D}k_{cat}$ value for PGHS-1 ranged from 1.8 to 2.3 with the three deuterated substrates. PGHS-2 was examined with only 10, 10, 13, 13-d_4-AA and exhibited a $^{D}k_{cat}$ value of 1.6. $^{D}K_M$ values ranged from 0.8 to 1.5 (Table 1), suggesting that each enzyme had roughly comparable affinities for unlabeled and deuterated AAs.

The KIE of k_{cat} varied little over the pH range of 6.2 to 8.2 (Table S1 in Supporting Information) and little solvent KIE was observed in the same pH range (Fig. S1 in Supporting Information). It should be noted, however, that both PGHS-1 and PGHS-2 exhibited larger KIE values at 30 °C (Table S1) than at 20 °C (Table 1). KIEs are generally expected to increase with decreasing temperature [25], and the basis for the unusual temperature dependence of the PGHS-1 and -2 KIEs is being investigated further.

3.2 PGHS-1 deuterium KIE from RFQ-EPR kinetics

Measurements of Tyr385· formation kinetics were made by reacting PGHS-1 anaerobically with EtOOH in control RFQ-EPR experiments (Fig. 2A). A 34 G WD1 EPR signal formed within 10 ms, similar to previous observations under aerobic conditions [26]. The line-shape gradually converted to a 32 G wide singlet (WS1) by ~5 s. When EtOOH was reacted anaerobically with PGHS-1 pre-equilibrated with AA or 13, 13-d_2-AA, the WD1 EPR signal intensity was maximal at the first time point (10 ms) and decayed subsequently (Figs. 2B and 2C). The WD1 was replaced by a 24 – 25 G narrow singlet without displaying the wide singlet feature (WS1) observed in the absence of fatty acid. The lineshape of this narrow singlet was essentially the same as the NS1c tyrosyl radical (Tsai et al., accompanying paper in this issue).

In the control reactions without fatty acid the total radical intensity (WD1 + WS1) increased at a rate of ~55 s^{-1} to reach a maximum of ~0.3 spin/heme at 100 ms, changed little for several seconds, and then decayed slowly at a rate ~ 0.01 s^{-1} (Fig. 3). To examine the radical kinetics for reactions of EtOOH with PGHS-1 pre-equilibrated with fatty acid, the EPR spectra in panels B and C of Fig. 2 were resolved into WD1 and NS1c components using the spectral deconstruction approach (Experimental Procedures). The intensities of the resulting WD1 and NS1c components are shown as a function of reaction time in Fig. 3. WD1 intensity was maximal at the first time point for reactions with unlabeled and deuterated AAs, and subsequently decayed at 25 s^{-1} for AA and more slowly (18 s^{-1}) for reactions with 13, 13-d_2-AA. NS1c signal intensities increased at a slight slower rate than found for decay of WD1 intensities (Fig. 3). The rate constants for NS1c formation were 14

NIH-PA Author Manuscript

NIH-PA Author Manuscript

NIH-PA Author Manuscript

± 3 s^{-1} (n = 3) for reactions with AA and 7 ± 3 s^{-1} (n = 3) for reactions with 13, 13-d_2-AA, giving a KIE value for NS1c formation of 2.0 ± 1.3 (n = 3). The intensity of the NS1c radical decayed slowly (~0.08 s^{-1}) for reactions with unlabeled or deuterated AA (Fig. 3).

The RFQ-EPR spectra in panels B and C of Fig. 2 were separately resolved into WD1 and NS1c components by global analysis based on the model in Eq. IX (Experimental Procedures) (Fig. 4). The resulting rate constants for NS1c radical formation were 16 ± 8 s^{-1} with AA as substrate, and 10 ± 4 s^{-1} with 13, 13-d_2-AA as substrate. The KIE value calculated from these rate constants was 2 ± 1.

Global analysis of the RFQ-EPR spectra in Fig. 2 was also performed with a three-step model with an AA radical intermediate between WD1 and NS1c (data not shown). This analysis attributed very little intensity to the AA radical, and the corresponding resolved EPR spectrum was much narrower than the EPR of an authentic pentadienyl radical. Thus, global analysis indicated that little if any AA pentadienyl radical signal is present in the RFQ-EPR spectra in Fig. 2, corroborating the results from spectral deconstruction.

3.3 Computer modeling to estimate intrinsic KIE values for the hydrogen transfer step(s)

Computer simulation of radical kinetics provides a way to estimate the intrinsic KIE for the H-transfer step (*A* in Scheme 1) based on the NS1c formation kinetics determined by RFQ EPR measurements. As depicted in Scheme 2, the radical interconversions occurring during anaerobic reaction of EtOOH with AA and PGHS can be described by a simple three-step model:

$$\text{Y385}\cdot + \text{AA} \overset{k_1}{\longleftrightarrow} \text{Y385+AA}\cdot \overset{k_2}{\longleftrightarrow} \text{AA+NS1c} \overset{k_3}{\longrightarrow} \text{EPR silent species} \qquad \text{[Eq. XI]}$$

This model is essentially an expansion of that used for global analysis of the RFQ-EPR data (Eq. IX) to explicitly include the hydrogen transfer step that forms the pentadienyl AA radical (AA). Predictions of reaction time courses expected for the mechanism in Eq. XI were obtained by simulations with SCoP using the parameter set mentioned in Experimental Procedures. We first assessed the sensitivity of the pentadienyl AA radical kinetics to the value of k_2, fixing k_1 and k_3 close to the observed values for NS1c formation and decay, respectively. The proportion of pentadienyl AA radical accumulation was predicted to be very sensitive to the value of k_2 (Fig. 5). When k_2 was set at 50 s^{-1}, 2.5 times the value of k_1, AA radical accumulation was predicted to peak at ~20% of the initial concentration of WD1 (Fig. 5A). When k_2 was set at 200 s^{-1}, accumulation of AA radical decreased to less than 10% of the initial level of WD1 (Fig. 5B). Increasing k_2 to 500 s^{-1} further decreased the predicted peak level of AA radical (Fig. 5C). As noted above, a pentadienyl radical component was not resolved from the RFQ-EPR data by either spectral deconstruction or global analysis. In practice, an AA pentadienyl radical accounting for 10% or less of total spin would be very difficult to resolve from the WD1 and NS1c radical signals. All of this strongly suggests that a rate constant for hydrogen transfer to AA radical (k_2) of ≥ 200 s^{-1} is quite reasonable, and indeed the kinetic data for WD1 and NS1c determined by RFQ-EPR were well simulated with $k_2 \geq 200$ s^{-1} (Fig. 5B).

The observed KIE, ^{D}k, in RFQ-EPR presumably reflects a combination of k_1, k_{-1}, k_2, k_{-2} and k_3, with k_1 and k_2 as dominant parameters. The hydrogen atom transferred between AA/AA and Tyr385/Tyr385 in step 1 is replaced by deuterium in the labeled substrate, so both forward and reverse kinetics of this step should be slower with the deuterated AA. Two scenarios can be envisioned for step 2. If NS1c is on Tyr385', formation of the NS1c radical (step 2) will involve transfer of the hydrogen/deuterium atom originally removed from C13 of AA in step 1, and thus step 2 kinetics also should be slowed with the labeled substrate.

NIH-PA Author Manuscript

NIH-PA Author Manuscript

NIH-PA Author Manuscript

On the other hand, if the NS1c tyrosyl radical forms on a residue other than Tyr385 (e.g., Tyr348), only protium transfers would be involved in step 2 and the kinetics of this step would be insensitive to AA deuteration.

Simulations were first performed for the case where AA deuteration affects only the kinetics of step 1. For each specific k_2 value, the generated kinetic trace for NS1c formation could be fitted to Eq. X to get a predicted rate, k_{pred}. When k_2 was 200 s^{-1} or faster, the predicted KIE, calculated as the ratio of the k_{pred} using AA or to that with 13, 13-d_2-AA as substrate, ($k_{pred,\ AA}/k_{pred,\ d2\text{-}AA}$), leveled off at 1.85, about 7.5% lower than the preset intrinsic KIE ($k_{1,\ AA}/k_{1,\ d2\text{-}AA}$), 2.0 (Fig. 6A). The simulation also predicted that when $k_2 \gg k_1$, the predicted KIE was directly proportional to the preset intrinsic KIE (Fig. 6B). This linear relationship indicates that the ratio of NS1c formation rates with AA and 13, 13-d_2-AA approximate the actual intrinsic KIE for hydrogen abstraction from AA. Combining the results from RFQ-EPR analysis and computer modeling, we estimate the intrinsic KIE of C13 *pro-(S)* hydrogen abstraction from AA by Tyr385· to be 2.3 (spectral synthesis method) or 1.9 (global analysis).

For simulations of the case where the kinetics of both step 1 and 2 are affected by AA deuteration, we set the intrinsic KIE of step 1 equal to that of step 2. The predicted KIE values in this case were almost independent of the k_2 value chosen, and ranged between 1.88 and 1.91, slightly lower than the preset KIE value of 2.0 (Fig. 6A). The predicted KIEs for NS1c formation exhibited an approximately linear relationship with the set intrinsic KIE, when the latter was lower than 6 and $k_2 \geq k_1$ (Fig. 6B). When the preset intrinsic KIE value was > 6, the predicted KIE for NS1c formation rose sharply (Fig. 6B), suggesting that the overall KIE can be significantly larger than the intrinsic KIE of either step when both steps are isotope sensitive. However, the overall KIE values observed in the RFQ-EPR experiments were ~2, well below the predicted threshold for non-linear behavior (Fig. 6B). Thus, the simulation results suggest that the KIE for formation of NS1c is a good approximation of the intrinsic KIE for hydrogen transfer from AA to Tyr385· when the first two steps in the mechanism are both isotope sensitive.

4. DISCUSSION

The results from the present non-competitive, steady-state measurements show that PGHS-1 and -2 have primary deuterium KIEs in the range of 1.7 – 2.3 for cyclooxygenase catalysis. The current data do not permit calculation of a secondary KIE for *pro-(R)* deuterium substitution at C13. The observed primary deuterium $^{D}k_{cat}$ values are considerably smaller than the theoretical maximum of 7–8 [27], which could be due to other steps masking a larger intrinsic isotope effect. The small $^{D}(k_{cat}/K_M)$ values may result from the dissociation of the PGHS(AA) reaction complex being significantly slower than AA conversion to PGG_2. One aspect that may affect the cyclooxygenase isotope effect is reversibility of *pro-(S)* hydrogen abstraction from C13 of AA (step A in Scheme 1). Such reversibility was inferred from the observation of a competitive ^{18}O KIE, which indicates that O_2 addition occurs in or before the first kinetically irreversible step [14]. Based on the magnitude of the measured competitive ^{18}O KIE, the first kinetically irreversible step was proposed to be either endoperoxide formation or formation of the bicyclic intermediate (Scheme 1, steps C and D, respectively) [14]. On the other hand, the calculated free energy surface for PGG_2 formation suggested that two other steps have considerable activation energies: 14.5 kcal/mol for C13 *pro-(S)* hydrogen abstraction and 14.9 kcal/mol for cyclopentane ring closure [28]. Both of these steps were expected to be irreversible due to the large activation energy barriers for the reverse reactions, 23.7 and 23.6 kcal/mol, respectively [28].

NIH-PA Author Manuscript

NIH-PA Author Manuscript

NIH-PA Author Manuscript

To evaluate whether the small primary deuterium KIEs measured for steady state turnover reflect the intrinsic KIE of the hydrogen abstraction step, we attempted to directly measure the kinetics of AA radical formation in PGHS-1 with AA and C13 *pro*-(*S*) deuterated AA as substrate. Based on the current mechanism (Scheme 1), we expected to isolate the C13 *pro-(S)* hydrogen abstraction step from subsequent steps under anaerobic conditions. However, we found that the AA radical did not accumulate even in the absence of O_2 but was converted rapidly to another tyrosyl radical, NS1c (Fig. 2) (Tsai et al., accompanying paper in this issue) and no experimental evidence suggested that this conversion was a multi-step process. Although the AA pentadienyl radical EPR signal was not evident in the RFQ-EPR data, the involvement of a transient AA radical intermediate was demonstrated by the faster formation of NS1c with AA than with 13,13-d_2-AA (Fig. 3). Direct conversion of WD1 to NS1c should not produce a deuterium KIE. Furthermore, an AA pentadienyl radical intermediate itself was observed when PGHS-1 was reacted with a mixture of AA and EtOOH, rather than being pre-equilibrated with AA before reaction with EtOOH (Tsai et al., accompanying paper in this issue). Additional indication of an AA radical intermediate between WD1 and NS1c comes from the observation that WD1 decay was faster than NS1c formation for both AA and 13, 13-d_2-AA substrates (Fig. 3). Further support for the AA radical as a precursor to NS1c (as depicted in Scheme 2) is the observed formation of an oxime adduct at C11 of AA when NO was used as a radical trapping agent under conditions that generate NS1c (Lü et al., accompanying paper in this issue). Our interpretation is that NO trapped an AA radical that is in equilibrium with NS1c (Scheme 2). O_2 may similarly drive cyclooxygenase reactions downstream from the initially formed AA radical to form PGG_2 (Scheme 1).

The projected hydrogen transfer from tyrosine to AA pentadienyl radical to form NS1c (Scheme 2) would seem to be thermodynamically uphill given the redox potentials for model pentadienyl and tyrosyl radical species (~0.6 and ~0.9 V, respectively [29,30]. However, these midpoint potentials may be significantly shifted when the radical intermediates are in the PGHS active site environment. For example, a slight steric constraint exerted by the protein could easily convert the pentadienyl radical to an allyl radical, whose redox potential can be above 0.9 V [29]. Similarly, the redox potential of the NS1c tyrosyl radical could be lowered if the radical is stabilized by local H-bonding and polarity changes. A drop of just 100 mV for the latter half reaction would make the thermodynamics favorable for NS1c formation. Lysine 2,3-amino mutase provides an example of redox potential modulation by the protein environment [31]. In this case, the reversible, hemolytic cleavage of S-adenosyl methionine (SAM) involves electron transfer from the [4Fe-4S] iron-sulfur center to the sulfonium group of SAM, theoretically an uphill process. However, binding of substrate lysine was found to decrease the midpoint potential of the [4Fe-4S] center by 0.17 V and the equilibrium constant of the reaction indicates that binding to the iron-sulfur cluster increases SAM's redox potential by 0.73 V.

The absence of AA radical accumulation in our RFQ-EPR experiments provided a constraint on the k_2/k_1 ratio in our computer modeling (Fig. 5), and suggests that the NS1c formation rate is approximately an order of magnitude faster than the initial hydrogen transfer from AA to Tyr385· (Fig. 6A). Simulations with a k_2/k_1 ratio of 10 predicted a KIE for NS1c formation that was slightly lower than the preset intrinsic KIE of the first hydrogen abstraction (Fig. 6A). In other words, the KIE value experimentally determined for NS1c radical formation approximates the intrinsic KIE value for the hydrogen transfer step. Analysis of the RFQ-EPR kinetic data by two separate approaches resulted in KIE values between 1.9 and 2.3. Thus, the KIE value for hydrogen abstraction from AA by Tyr385· is likely to be ~2. The similarity between the estimated hydrogen abstraction KIE value and the $^{D}k_{cat}$ values determined by steady-state kinetics indicates that the non-competitive $^{D}k_{cat}$ is not suppressed noticeably by the kinetic complexity of the cyclooxygenase reaction and

NIH-PA Author Manuscript

NIH-PA Author Manuscript

NIH-PA Author Manuscript

that a hydrogen abstraction step is partially rate-limiting in cyclooxygenase catalysis, along with the first O_2 insertion and bi-cyclic ring formation. Rate limitation at the hydrogen abstraction step is also consistent with the earlier observation of accumulation of the WD1 tyrosyl radical when AA was mixed with PGHS-1 in the presence of excess oxygen [32].

The minimal observed effect of pH on the KIE of k_{cat} and the lack of solvent deuterium KIE in the steady-state kinetic measurements (Table S1 and Fig. S1) indicate that there is no additional chemical step involving the participation of a pH-sensitive amino acid side chain or the proton exchange with the solvent in our observed KIE. Thus our proposed mechanism in Scheme 2 including two chemical steps: WD1 → AA pentadienyl radical → NS1c provides a minimal model to account for both steady-state and pre-steady state kinetic data.

The modest deuterium KIEs of ~2 observed with PGHS-1 and -2 are in sharp contrast to the extremely large KIEs observed with plant lipoxygenases (LOX), e.g., 65 for linoleic acid [33–37] and 97 for AA [38]. These non-heme iron enzymes also catalyze fatty acid dioxygenation, and the LOX mechanism also appears to involve generation of a substrate radical before oxygen incorporation [39–41]. In the LOX mechanism, peroxide reacts with the ferrous form of the enzyme, generating a ferric intermediate that abstracts hydrogen from the fatty acid substrate to generate a substrate radical and Fe(II)-OH_2. Addition of O_2 to the fatty acid radical leads to a peroxyl radical, which reacts with Fe(II)-OH_2 to form hydroperoxy fatty acid and regenerates Fe(III)-OH to start another catalytic cycle. Many studies have found that hydrogen transfer from fatty acid substrate is the overall rate-determining step for LOX catalysis [33–37]. The large KIEs observed for LOX have been attributed to quantum hydrogen tunneling [33–37]. The striking difference between LOX and PGHS-1 and -2 in the KIE for hydrogen abstraction indicates that the structures of the transition complexes ([Fe(III)-OH --- H --- AA] for LOX and [Tyr385 --- H --- AA] for PGHS) are very different.

Intrinsic deuterium KIEs significantly less than the theoretical maximum of 7 – 8 predicted by absolute rate theory [27] have been reported for various reactions [42–44]. Kinetic isotope effect of a reaction reaches the classical limit only for symmetrical transition state, but becomes smaller when it resembles more like either the product or the reactant. The very small cyclooxygenase KIE indicates that the structure of the activation complex in PGHS-1 or PGHS-2, [Tyr385· --- H --- AA], is very asymmetric, biased towards either reactants or products. The calculated free energy surface of this step suggests the bias is probably towards the reactant side [28].

In summary, our steady-state and pre-steady state deuterium KIE studies provide strong evidence for the rate-limiting nature of the first hydrogen transfer step of cyclooxygenase catalysis. Our strategy in binding AA to the PGHS before reaction with EtOOH anaerobically by RFQ/EPR constrained our rate determination in only two chemical steps, including first a H-transfer between AA and Tyr and a second rapid equilibrium between AA and the tyrosine that forms NS1c. The latter fast radical equilibrium was concluded from the studies of the other two accompanying papers. Computer modeling based on the minimal mechanism with these two chemical steps enabled determination of the intrinsic rate of the H-transfer. Such powerful and innovative approach is new in the literature and could find useful application in resolving intrinsic rate and the associated KIE for other enzyme systems. The observation that the cyclooxygenase KIE is more than an order of magnitude less than that for non-heme iron lipoxygenases indicates that the two types of fatty acid oxygenase have very different underlying mechanisms for the H-transfer step.

NIH-PA Author Manuscript

NIH-PA Author Manuscript

NIH-PA Author Manuscript

Supplementary Material

Refer to Web version on PubMed Central for supplementary material.

Acknowledgments

Supported by NIH GM44911 (A.-L.T), and GM52170 (R.J.K).

5. ABBREVIATIONS

PGHS-1 and -2	prostaglandin H synthase isoforms 1 and 2
PGG_2	prostaglandin G_2
AA	arachidonic acid
13-*pro*-(*S*) d-AA, 13	13-d_2-AA, and 10, 10, 13,13-d_4-AA, arachidonic acid with deuterium substitution on C13 and/or C10
EtOOH	ethyl hydrogen peroxide
KIE	kinetic isotope effect
EPR	electron paramagnetic resonance spectrometry
WD1	wide doublet tyrosyl radical EPR signal in PGHS-1
NS1c	narrow singlet tyrosyl radical EPR signal in PGHS-1 reacted anaerobically with EtOOH and AA
RFQ	rapid freeze quench

References

1. Shimokawa T, Kulmacz RJ, Dewitt DL, Smith WL. J Biol Chem 1990;265:20073–20076. [PubMed: 2122967]
2. Tsai AL, Kulmacz RJ. Prostagl Other Lipid Mediat 2000;62:231–254.
3. Kiefer JR, Pawlitz JL, Moreland KT, Stegeman RA, Hood WF, Gierse JK, Stevens AM, Goodwin DC, Rowlinson SW, Marnett LJ, Stallings WC, Kurumbail RG. Nature 2000;405:97–101. [PubMed: 10811226]
4. Rouzer CA, Marnett LJ. Chem Rev 2003;103:2239–2304. [PubMed: 12797830]
5. Tsai AL, Kulmacz RJ. Arch Biochem Biophys 2009;493:103–124. [PubMed: 19728984]
6. van der Donk WA, Tsai AL, Kulmacz RJ. Biochemistry 2002;41:15451–15458. [PubMed: 12501173]
7. Hamberg M, Samuelsson B. J Biol Chem 1967;242:5336–5343. [PubMed: 6070851]
8. Peng S, Okeley NM, Tsai AL, Wu G, Kulmacz RJ, van der Donk WA. J Am Chem Soc 2002;124:10785–10796. [PubMed: 12207535]
9. Tsai AL, Hsi LC, Kulmacz RJ, Palmer G, Smith WL. J Biol Chem 1994;269:5085–5091. [PubMed: 8106487]
10. Tsai AL, Palmer G, Xiao G, Swinney DC, Kulmacz RJ. J Biol Chem 1998;273:3888–3894. [PubMed: 9461572]
11. Tsai AL, Kulmacz RJ, Palmer G. J Biol Chem 1995;270:10503–10508. [PubMed: 7737984]
12. Karthein R, Dietz R, Nastainczyk W, Ruf HH. Eur J Biochem 1988;171:313–320. [PubMed: 2828053]
13. Tsai AL, Wu G, Palmer G, Bambai B, Koehn JA, Marshall PJ, Kulmacz RJ. J Biol Chem 1999;274:21695–21700. [PubMed: 10419480]
14. Mukherjee A, Brinkley DW, Chang KM, Roth JP. Biochemistry 2007;46:3975–3989. [PubMed: 17355126]

NIH-PA Author Manuscript

NIH-PA Author Manuscript

NIH-PA Author Manuscript

15. Brill AS, Williams RJ. Biochem J 1961;78:253–262. [PubMed: 16748874]
16. Peng S, Okeley NM, Tsai AL, Wu G, Kulmacz RJ, van der Donk WA. J Am Chem Soc 2001;123:3609–3610. [PubMed: 11472139]
17. Peng S, Okeley NM, Tsai AL, Wu G, Kulmacz RJ, van der Donk WA. J Am Chem Soc 2002;124:10785–10796. [PubMed: 12207535]
18. Jacquot C, Wecksler AT, McGinley CM, Segraves EN, Holman TR, van der Donk WA. Biochemistry 2008;47:7295–7303. [PubMed: 18547056]
19. Peng S, McGinley CM, van der Donk WA. Org Lett 2004;6:349–352. [PubMed: 14748590]
20. Kulmacz RJ, Tsai AL, Palmer G. J Biol Chem 1987;262:10524–10531. [PubMed: 3038886]
21. Kulmacz RJ, Palmer G, Tsai AL. Mol Pharmacol 1991;40:833–837. [PubMed: 1658613]
22. Kulmacz, RJ.; Lands, WEM. Prostaglandins and Related Substances: A Practical Approach. Benedetto, C.; McDonald-Gibson, RG.; Nigam, S.; Slater, TF., editors. IRL Press; Washington, DC: 1987. p. 209-227.
23. Colen AH, Wilkinson RR, Fisher HF. J Biol Chem 1975;250:5243–5246. [PubMed: 238982]
24. Tsai AL, Berka V, Kulmacz RJ, Wu G, Palmer G. Anal Biochem 1998;264:165–171. [PubMed: 9866678]
25. Klinman JP. Philos Trans R Soc Lond B Biol Sci 2006;361:1323–1331. [PubMed: 16873120]
26. Tsai A, Wu G, Palmer G, Bambai B, Koehn JA, Marshall PJ, Kulmacz RJ. J Biol Chem 1999;274:21695–21700. [PubMed: 10419480]
27. Kresge, AJ. Isotope effects on enzyme-catalyzed reactions. Cleland, WW.; O'Leary, MH.; Northrop, DB., editors. University Park Press; Baltimore: 1977. p. 37-63.
28. Blomberg LM, Blomberg MRA, Siegbahn PEM, van der Donk WA, Tsai AL. J Phys Chem B 2003;107:3297–3308.
29. DeFelippis MR, Murthy CP, Faraggi M, Klapper MH. Biochemistry 1989;28:4847–4853. [PubMed: 2765513]
30. Koppenol WH. FEBS Lett 1990;264:165–167. [PubMed: 2358063]
31. Frey PA, Hegeman AD, Reed GH. Chem Rev 2006;106:3302–3316. [PubMed: 16895329]
32. Tsai AL, Palmer G, Kulmacz RJ. J Biol Chem 1992;267:17753–17759. [PubMed: 1325448]
33. Glickman MH, Klinman JP. Biochemistry 1995;34:14077–14092. [PubMed: 7578005]
34. Glickman MH, Klinman JP. Biochemistry 1996;35:12882–12892. [PubMed: 8841132]
35. Jonsson T, Glickman MH, Sun SJ, Klinman JP. J Am Chem Soc 1996;118:10319–10320.
36. Glickman MH, Wiseman JS, Klinman JP. J Am Chem Soc 1994;116:793–794.
37. Hwang CC, Grissom CB. J Ame Chem Soc 1994;116:795–796.
38. Peng S, van der Donk WA. J Am Chem Soc 2003;125:8988–8989. [PubMed: 15369335]
39. Andreou A, Feussner I. Phytochemistry 2009;70:1504–1510. [PubMed: 19767040]
40. Hamberg M, Samuelsson B. J Biol Chem 1967;242:5329–5335. [PubMed: 6070850]
41. Rickert KW, Klinman JP. Biochemistry 1999;38:12218–12228. [PubMed: 10493789]
42. Denu JM, Fitzpatrick PF. Biochemistry 1994;33:4001–4007. [PubMed: 7908225]
43. Balasubramanian B, Pogozelski WK, Tullius TD. Proc Natl Acad Sci U S A 1998;95:9738–9743. [PubMed: 9707545]
44. Baciocchi E, Lanzalunga O, Manduchi L. Chem Commun. 1999

NIH-PA Author Manuscript

NIH-PA Author Manuscript

NIH-PA Author Manuscript

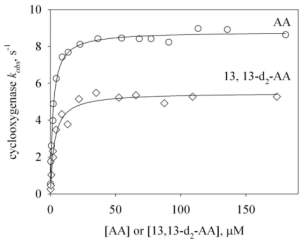

Figure 1. Substrate dependence of PGHS-2 cyclooxygenase activity with AA (circles) and 13, 13-d_2-AA (diamonds)

The cyclooxygenase rates were measured at 20 °C and pH 7.2. The lines represent the fits to the Michaelis-Menten equation. This substrate dependence of activity is one out of three complete experiments which yielded similar results.

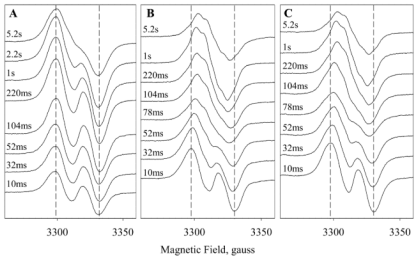

Figure 2. RFQ-EPR spectral changes during anaerobic reactions of EtOOH with PGHS-1 alone (panel A), PGHS-1 pre-equilibrated with AA (panel B) or PGHS-1 pre-equilibrated with 13, 13-d_2-AA (Panel C)

The RFQ reactions used 30 μM PGHS-1, 150 μM fatty acid and 150 μM EtOOH. The reaction time is indicated on each spectrum. The vertical dashed lines indicate the positions of the peak and trough of the earliest WD1 spectrum, providing a visual guide for later changes in linewidth. Two additional repetitions of such RFQ-EPR kinetic measurements gave similar outcome.

NIH-PA Author Manuscript
NIH-PA Author Manuscript
NIH-PA Author Manuscript

NIH-PA Author Manuscript

NIH-PA Author Manuscript

NIH-PA Author Manuscript

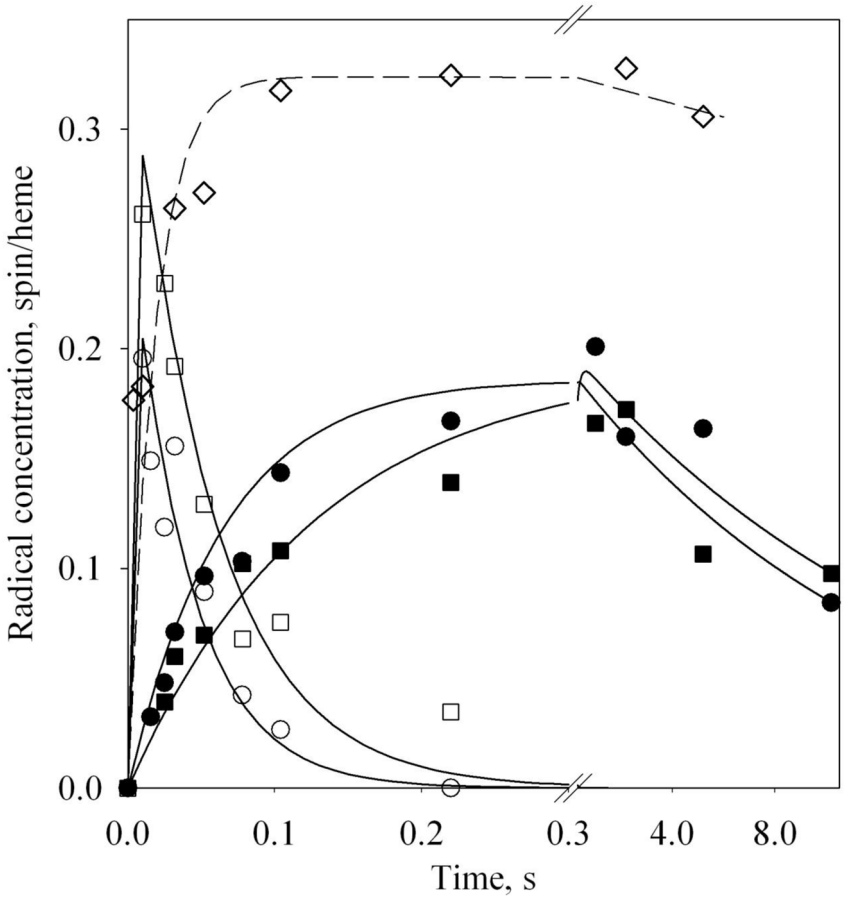

Figure 3. Effects of AA deuteration on the kinetics of WD1 and NS1c radical species during anaerobic reaction of PGHS-1 with fatty acid and peroxide

Analysis of the EPR spectra in Fig. 2 by spectral resolution was used to evaluate the concentrations of WD1 (open symbols) and NS1c (filled symbols) during reactions of EtOOH with PGHS-1 pre-equilibrated with AA (circles) or 13, 13-d_2-AA (squares). Solid lines are the fits to [Eq. VIII] for each resolved radical species. The kinetic data of tyrosyl radical (diamonds) and its fit to [Eq. VIII] (dashed line) in the control reaction of PGHS-1 with EtOOH are also shown. Similar outcome of the WD1 and NS1c kinetics were also obtained from other two complete sets of experiments.

NIH-PA Author Manuscript

NIH-PA Author Manuscript

NIH-PA Author Manuscript

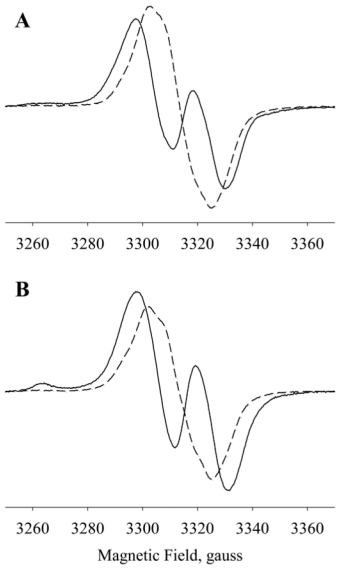

Figure 4. EPR signatures of radical intermediates resolved by global analysis

The sets of RFQ-EPR spectra obtained during anaerobic reaction of EtOOH (150 μM) with PGHS-1 (30 μM) pre-equilibrated with 150 μM AA or 13, 13-d_2-AA (panels B and C of Fig. 2) were analyzed by global analysis using a two-step model (Eq. IX). The resulting resolved EPR spectra for WD1 (solid lines) and NS1c (dashed lines) are shown for reactions with AA (panel A) and with 13, 13-d_2-AA (panel B). Details are described in Experimental Procedures. Essentially identical resolved component spectra were also obtained from other two sets of experiments.

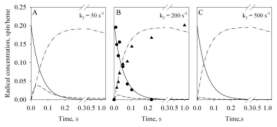

Figure 5. Computer simulated kinetics of radicals in the anaerobic reactions of EtOOH with PGHS-1 pre-equilibrated with AA

Simulations are shown in solid line for WD1, dash-dot-dot line for AA pentadienyl radical, and dash line for NS1c. Rate constants used in the simulations: k_1, 20 s^{-1}; k_{-1}, 0 s^{-1}; k_2 50 s^{-1} (panel A), 200 s^{-1} (panel B) or 500 s^{-1} (panel C); k_{-2}, 1 s^{-1}; and k_3, 0.08 s^{-1}. The comparison of WD1 and NS1c kinetics from RFQ-EPR of EtOOH reacted with PGHS-1 pre-equilibrated with AA (from Fig. 4) with the simulated kinetics of tyrosyl radicals is shown in Panel B. Solid circles, WD1 radical; solid triangles, NS1c radical.

NIH-PA Author Manuscript NIH-PA Author Manuscript NIH-PA Author Manuscript

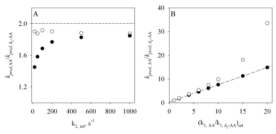

Figure 6. KIE predicted from simulated kinetic data

Panel A: dependence of the predicted KIE (= $k_{pred,\ AA}/k_{pred,\ d2\text{-}AA}$) on value of k_2, with k_1 = 20 s^{-1} (for AA) or 10 s^{-1} (for d_2-AA). Solid circles: k_2 = 20 – 1000 s^{-1} for both AA and d_2-AA; open circles: k_2 = 20 – 1000 s^{-1} for AA and $k_{2,\ AA}/k_{2,\ d2\text{-}AA}$ = 2. The value of preset intrinsic KIE, $k_{1,\ AA}/k_{1,\ d2\text{-}AA}$ = 2, is marked with the dashed line. Panel B: correlation between predicted KIE, $k_{pred,\ AA}/k_{pred,\ d2\text{-}AA}$, and preset intrinsic KIE, $k_{1,\ AA}/k_{1,\ d2\text{-}AA}$, with k_1= 20 s^{-1} (AA) or 1 – 20 s^{-1} (d_2-AA). Solid circles: k_2 = 200 s^{-1} for both AA and d_2-AA; open circles: k_2, 20 – 1000 s^{-1} for AA and $k_{2,\ AA}/k_{2,\ d2\text{-}AA} = k_{1,\ AA}/k_{1,\ d2\text{-}AA}$. For all the simulations, k_3 = 0.08 s^{-1}; k_{-2} = 1 s^{-1}; k_{-1}, 0 s^{-1}.

NIH-PA Author Manuscript NIH-PA Author Manuscript NIH-PA Author Manuscript

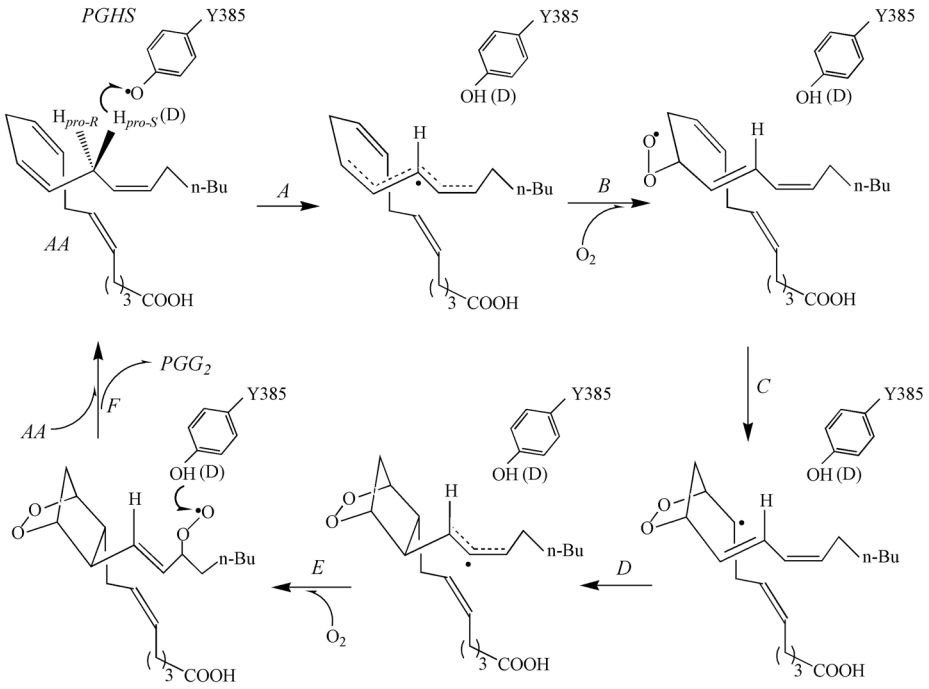

Scheme 1. Mechanistic model for cyclooxygenase catalytic cycle based on the proposal by Hamberg and Samuelsson [7]

"D" represents the deuterium substitution that produces the primary KIE. Two hydrogen abstraction steps could be sensitive to AA deuteration (marked by thick arrows): abstraction of C13 *pro-(S)* hydrogen by Tyr385· (step *A*) and abstraction of hydrogen from Tyr385 by the PGG_2 radical (step *F*). The reversibility of individual reaction steps has not been confirmed and therefore is not shown. Tyr385 is assumed to be kinetically inactive in the O_2 insertion steps (*B* and *E*) and the AA double bond rearrangement steps (*C* and *D*).

NIH-PA Author Manuscript NIH-PA Author Manuscript NIH-PA Author Manuscript

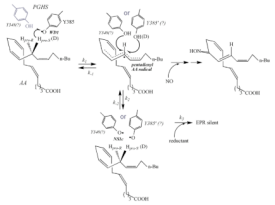

Scheme 2. Proposed interconversions of radical intermediates during anaerobic reaction of PGHS with peroxide and AA

Left: the initial Tyr385 radical species (WD1) with bound AA (labeled or unlabeled). Center, top: pentadienyl AA radical species bound in active site with ground state Tyr348 and Tyr385 nearby; Tyr385 ring in relaxed conformation. Center, bottom: NS1c tyrosyl radical species involving Tyr348 or Tyr385 with relaxed conformation. Hydrogen transfers for k_1 and k_2 steps are indicated by thick arrows. The NS1c tyrosyl radical reacts with reductant to form EPR silent species in the k_3 step. Addition of NO as a radical trapping agent, has been found to rapidly form an NO-AA adduct (Lü et al., accompanying paper in this issue).

NIH-PA Author Manuscript NIH-PA Author Manuscript NIH-PA Author Manuscript

NIH-PA Author Manuscript NIH-PA Author Manuscript NIH-PA Author Manuscript

Table 1

PGHS-1 and -2 cyclooxygenase kinetic parameters and non-competitive KIEs for reaction at 20 °C and pH 7.2.[1]

PGHS	k_{cat}, s^{-1}	K_M, μM	k_{cat}, s^{-1}	K_M, μM	Deuterium Kinetic Isotope Effect		
					$^{D}k_{cat}$	$^{D}K_M$	$^{D}(k_{cat}/K_M)$
	AA		*13 pro-(S) d_1-AA*				
PGHS-1*	44.6 ± 0.8	5.4 ± 0.4	24 ± 1	3.5 ± 0.8	1.8 ± 0.2	1.5 ± 0.5	1.2 ± 0.5
	AA		*13, 13-d_2-AA*				
PGHS-1	20.8 ± 0.7	6.4 ± 0.8	8.9 ± 0.3	4.6 ± 0.7	2.3 ± 0.2	1.4 ± 0.4	1.6 ± 0.6
PGHS-2	9.2 ± 0.4	2.3 ± 0.3	5.6 ± 0.1	2.8 ± 0.4	1.6 ± 0.1	0.8 ± 0.2	2.0 ± 0.6
	AA		*10, 10, 13, 13-d_4-AA*				
PGHS-1	57 ± 1	6 ± 1	31 ± 1	5.0 ± 0.9	1.8 ± 0.3	1.3 ± 0.5	1.4 ± 0.8

[1]Values indicate the mean ± average deviation from the mean obtained from two (*) or four experiments. Data in the same row were generated from the same batch of enzyme and batch to batch activity variation was noticed.

KIEs for 13 *pro*-(*S*) d_1-AA and 10, 10, 13 13-d_4-AA were measured using a high sensitivity electrode membrane; those for 13, 13-d_2-AA were measured using a standard sensitivity membrane.